Journal of Controlled Release 352 (2022) 1134–1143

Contents lists available at ScienceDirect

Journal of Controlled Release

journal homepage: www.elsevier.com/locate/jconrel

Effect of acoustic cluster therapy (ACT®) combined with chemotherapy in a patient-derived xenograft mouse model of pancreatic cancer

Serina Ng [a], Andrew John Healey [b], Per Christian Sontum [c], Svein Kvåle [b], Sverre H. Torp [d,e], Einar Sulheim [f,g], Daniel Von Hoff [a], Haiyong Han [a,*]

[a] Molecular Medicine Division, The Translational Genomics Research Institute (TGen), 445 N. Fifth Street, Phoenix, AZ, USA
[b] EXACT Therapeutics, Østre Aker vei 19, 0581 Oslo, Norway
[c] Bobler AS, Stålverkskroken 18, 0661 Oslo, Norway
[d] Department of Pathology and Medical Genetics, St. Olavs University Hospital, Trondheim, Norway
[e] Department of Laboratory Medicine, Children's and Women's Health, NTNU, Trondheim, Norway
[f] Department of Physics, Norwegian University of Science and Technology, Trondheim, Norway
[g] SINTEF Biotechnology and Nanomedicine, Trondheim, Norway

ARTICLE INFO

Keywords:
Acoustic cluster therapy
Microbubble
Pancreatic cancer
Ultrasound
Drug delivery

ABSTRACT

Pancreatic ductal adenocarcinomas respond poorly to chemotherapy, in part due to the dense tumor stroma that hinders drug delivery. Ultrasound (US) in combination with microbubbles has previously shown promise as a means to improve drug delivery, and the therapeutic efficacy of ultrasound-mediated drug delivery is currently being evaluated in multiple clinical trials. However, most of these utilize echogenic contrast agents engineered for imaging, which might not be optimal compared to specialized formulations tailored for drug delivery. In this study, we evaluated the in vivo efficacy of phase-shifting microbubble-microdroplet clusters that, upon insonation, form bubbles in the size range of 20–30 μm. We developed a patient-derived xenograft model of pancreatic cancer implanted in mice that largely retained the stromal content of the originating tumor and compared tumor growth in mice given chemotherapeutics (nab-paclitaxel plus gemcitabine or liposomal irinotecan) with mice given the same chemotherapeutics in addition to ultrasound and acoustic cluster therapy. We found that acoustic cluster therapy significantly improved the effect of both chemotherapeutic regimens and resulted in 7.2 times higher odds of complete remission of the tumor compared to the chemotherapeutics alone.

1. Introduction

Pancreatic ductal adenocarcinoma (PDAC) has a five-year survival rate of only approximately 9%, making it one of the most lethal malignancies, and its incidence is increasing [1]. In the USA, pancreatic cancer accounts for 3% of all cancers, but results in about 7% of all cancer deaths, making it the third leading cause of death due to cancer [2,3]. Some researchers have predicted that pancreatic cancer will become the second leading cause of cancer deaths in the USA by 2030 [4].

PDACs are notoriously resistant to conventional and targeted therapeutic agents. First-line standard-of-care (SoC) chemotherapy regimens for patients with advanced or metastatic PDAC consist of the cocktail FOLFIRINOX (oxaliplatin, irinotecan, 5-fluorouracil, leucovorin) or the combination of nab-paclitaxel plus gemcitabine, but these have only a modest improvement on the overall survival rate [5,6]. Liposomal irinotecan in combination with 5- fluorouracil and leucovorin was also approved by the USA Food and Drug Administration (FDA) for the treatment of patients with metastatic PDAC whose disease has progressed after gemcitabine-based chemotherapy [7]. A prerequisite for therapeutic benefit is that the active substance reaches its target pathology and that toxicity to healthy tissue and non-targeted organs is limited. Drug resistance in PDAC is thought to be strongly associated with stromal desmoplasia (proliferation of fibrotic tissues with an altered extracellular matrix - a hallmark of PDAC). The high stromal content of PDACs results in, amongst other effects, high interstitial fluid pressure causing a low rate of drug penetration into the tumor bed [8–13]. Modulating the tumor microenvironment to improve drug delivery, therefore, has the potential to provide a major impact on treatment outcomes of patients with PDAC. Studies have shown that reducing

* Corresponding author at: 445 N. Fifth St., Phoenix, AZ, USA.
E-mail address: hhan@tgen.org (H. Han).

https://doi.org/10.1016/j.jconrel.2022.11.016
Received 21 March 2022; Received in revised form 6 September 2022; Accepted 7 November 2022
Available online 21 November 2022

the stromal content in PDAC improves both drug delivery and therapeutic effect [14,15]. However, the effects of stroma and especially the possibility of overcoming this barrier to drug delivery using therapeutic ultrasound is poorly understood, partly because cell-line based xenograft tumor models generally exhibit a much lower stromal content than PDAC [16].

In recent years, ultrasound-mediated drug delivery has emerged as a technology with potential to locally increase drug delivery with quite encouraging results [17–21]. Most of these concepts explore the use of regular US contrast microbubbles such as SonoVue®, Optison™, or Definity®, either loaded with or co-injected with various active ingredients. The first human trial to evaluate the use of ultrasound to enhance drug delivery in pancreatic cancer tested gemcitabine combined with microbubbles and ultrasound in ten patients with inoperable pancreatic tumors [22]. Median survival (compared with a historical control) increased from 8.9 to 17.6 months, but study participants received 13.8 cycles of gemcitabine, making comparison to the historical control (8.3 cycles of gemcitabine) uncertain. More recently, ultrasound-mediated drug delivery has been evaluated in other cancers such as breast cancer [23] and glioblastoma [24]. Also, several Phase I/II studies are currently recruiting or being prepared (Clinicaltrials.gov NCT04146441, NCT04821284, NCT03477019 and NCT03458975).

Preclinically, ultrasound-mediated drug delivery using conventional microbubbles for imaging has been heavily investigated and has often shown promise. In one study using a human xenograft murine model of pancreatic cancer, an ultrasound-activated microbubble-liposome complex carrying irinotecan and oxaliplatin provided reductions in tumor size compared with the same concentration of irinotecan and oxaliplatin delivered conventionally [25]. Another ultrasound responsive microbubble formulation, this time loaded with 5-fluorouridine, irinotecan and oxaliplatin, resulted in pancreatic tumors that were 189% smaller compared with mice treated with a standard dose of FOLFIRINOX [26]. In a study using a complex of ultrasound-activated, doxorubicin-loaded magneto-liposome microbubbles in a pancreatic cancer xenograft model of nude mice, significant reductions in tumor volume were observed after intravenous administration of the microbubbles in comparison to the control group [27]. In mice with pancreatic tumors, pulsed high intensity focused ultrasound applied either before or during doxorubicin administration to induce localized inertial cavitation has been shown to disrupt the stromal matrix and increase the concentration of drug within the tumor [28]. A similar study combining high-intensity focused ultrasound and gemcitabine with microbubbles reported increased apoptosis rates and slower tumor growth with this regimen [29].

Despite these promising results, standard ultrasound contrast agents are designed and optimized for imaging and can have drawbacks that restrict their effectiveness in drug delivery. The small size of the microbubbles limits the potential magnitude of their effect and their free-flowing nature reduces the amount of contact they have with the endothelial wall and the amount of time that they remain within the tumor vasculature [30,31]. We hypothesize that bigger bubbles can perform greater biomechanical work onto the vascular wall and more efficiently permeate the vasculature and affect the extravascular space, leading to improved drug delivery to the sonicated region. Acoustic Cluster Therapy (ACT®) is a novel approach for ultrasound-mediated drug delivery which aims to address the limitations of drug delivery with standard contrast agents [32]. ACT® is a dispersion of clusters of negatively charged microbubbles and positively charged microdroplets. Following administration of ACT®, insonation is performed in a two-step process (Fig. 1). First, local, high frequency ultrasound activation causes the microbubbles to oscillate, inducing a phase shift of the microdroplet component from liquid to gas and the formation of large (approximately 22 μm diameter) bubbles [33]. These bubbles transiently lodge within the microvasculature of the insonated tissue (e.g. tumor). In the second phase, low frequency ultrasound is used to induce controlled volume oscillations that increase the local permeability of the vasculature and improve the distribution of the co-administered drug into the tumor [34,35].

Similar to the standard ultrasound insonation, ACT® aims to enhance the local permeability of the tumor vasculature, with the ultimate goal of increasing the extravasation, penetration and uptake of chemotherapeutic agents into the tumor tissues [36,37]. However, the larger size of the ACT® bubbles (1000× greater volume than standard contrast microbubbles) induces greater mechanical effects which extend further into the extravascular space compared to the smaller standard bubbles. Furthermore, the way the ACT® bubbles lodge within the microvasculature provides close contact with the endothelial wall for a prolonged period (5–10 min) while being retained in the capillary bed, further increasing effectiveness [32,37].

Safety assessments performed in dogs, rats and mice have demonstrated that ACT® is safe at doses up to 1 mL/kg when activated in the heart [38], liver [38], and brain [39,40]. Dogs exposed to ACT® at doses of 0.1–1.0 mL/kg, either with ultrasound applied to the heart for 1 min or with no ultrasound activation, showed no differences in observations of clinical signs, ophthalmoscopy, clinical pathology, macro-, and microscopy to animals who did not receive ACT® [38]. The only significant effects observed were a short-lasting reduction in circulating leukocytes and a reduction in platelets. Rats treated with ACT® at doses of 0.1–0.3 mL/kg, activated in the heart, showed no change in motor coordination. Also in rats, ACT® at doses of 0.1–1.0 mL/kg was activated in the liver for 5 min, with no subsequent effects on histopathology or clinical chemistry [38]. Finally, rats who received ACT® at a doses of 1 mL/kg with activation in the brain showed no clinically relevant histological changes [39]. In a recent study in mice who also received ACT® doses of 1 mL/kg with activation in the brain the histological evaluation showed no evidence of tissue damage, acute inflammatory response or haemorrhages [40].

To date, ACT® has improved drug delivery in cell-line xenograft

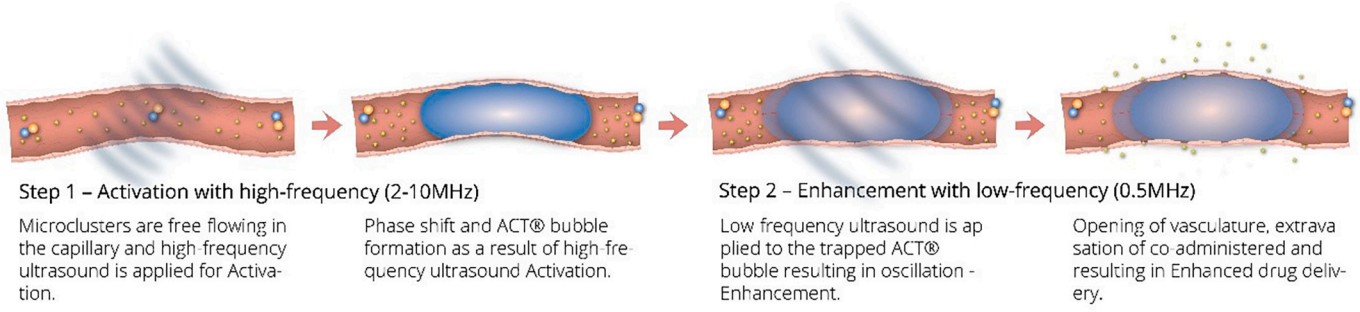

Fig. 1. Basic mechanism of ACT®. High frequency ultrasound activates the microbubble/microdroplet clusters within the targeted tumor (Step 1), causing the clusters to turn into a single large ACT® bubble, transiently trapped in the capillary bed. Low frequency ultrasound is then applied to make the ACT® bubble expand and contract (Step 2), leading to an increase in vascular permeability and enhanced drug delivery into the target tissue. ACT®, acoustic cluster therapy; US, ultrasound.

mouse models of prostate cancer [34,41], triple negative breast cancer [30], colon cancer [32], and PDAC [42]. However, these models are known to exhibit far less stroma than clinical PDAC. In this study we aimed to evaluate the effect of ACT® in combination with SoC in patient-derived xenograft (PDX) models that more accurately represent the histopathology and molecular features of the original tumor [43].

2. Materials and methods

2.1. ACT® compound and Sonazoid™

The ACT® drug product (PS101) is an aqueous dispersion of microbubble/microdroplet clusters. PS101clusters is prepared by reconstituting a freeze-dried powder containing microbubbles with 2 mL of an emulsion of microdroplets. The microbubbles are made of perfluorobutane (PFB) (16 μl/vial) stabilized by a monomolecular phospholipid membrane of hydrogenated egg phosphatidylserine (H-EPS) which is negatively charged. The microdroplet emulsion is made of perfluoromethylcyclopentane (PFMCP) (6.8 mg/mL) stabilized by a monomolecular distearoylphosphatidylcholine (DSPC) phospholipid membrane containing 3% (mol/mol) stearyl amine making the overall surface positively charged, dispersed in a 5 mM tris(hydroxymethyl) aminomethane (TRIS) buffer solution. The reconstituted PS101 formulation consists of approximately 6×10^7 clusters/mL with a median diameter of approximately 5 μm [37].

Sonazoid™ (GE Healthcare, Oslo, Norway) is a second-generation ultrasound contrast agent approved in several countries including Norway, Japan, Denmark, and South Korea for use in contrast-enhanced ultrasonography of focal liver and/or breast lesions [44]. Sonazoid™ is included in this study as a comparison to PS101.

2.2. Mice

Five-week old female athymic nude mice (Taconic Biosciences, Germantown, NY, USA) were used in this study. All animal experiments were approved by the Institutional Animal Care and Use Committee (IACUC) at the University of Arizona (Protocol #14–531), where the animal studies were carried out. All animal studies were performed adhering to recommendations in the Guide for the Care and Use of Laboratory Animals published by National Academies, USA.

2.3. Patient-derived xenograft model

PDX tumors were first established by subcutaneously implanting tumor chunks (4–8 mm^3) surgically removed from PDAC patients into the flanks of athymic nude mice. Once established, the tumors were subjected to whole-exome sequencing to verify that they retained the genetic alterations of the original patient tumor. Established PDX tumors were then propagated by subcutaneous implantation into new sets of mice and used in biological studies [45]. Briefly, tumors were cut into approximately 5 mm cubes and minced thoroughly using a scalpel. The minced tumor was then mixed with phosphate buffer saline (PBS, pH 7.4) to a volume of 1.5 mL per tumor cube. An equal volume of Matrigel was then added to the tumor solution and 150 μL of the mixture was implanted subcutaneously into each mouse. The PDX model used in this study was derived from a human PDAC tumor that harbored the *K-RAS*^{G12V} mutation. Mice were monitored for tumor growth and entered the study when tumor size reached between 120 and 200 mm^3.

2.4. Groups/treatment regimens

Mice entering the study were enrolled into one of seven treatment groups (9–10 mice/group, Table 1). Mice were stratified in the groups based on their tumor size to reduce the variability of tumor size distribution across the groups. On the same day, the mice were treated with saline and PS101, chemotherapeutics, chemotherapeutics in combination with (before or after) PS101 or chemotherapeutics followed by Sonazoid™. Gemcitabine (Gemzar®, Eli Lilly, Indianapolis, IN) was given intraperitoneally (IP) at a dose of 60 mg/kg, nab-paclitaxel (Abraxane®, Celgene, Summit, NJ) was given intravenously (IV) at a dose of 15 mg/kg, and liposomal irinotecan (Onivyde®, Ipsen Biopharm, Cambridge, MA) was given IV at a dose of 15 mg/kg. Liposomal irinotecan is a nanocarrier formulation of irinotecan encapsulated in negatively charged polyanionic liposomes [46]. The formulation has a particle size of liposomal irinotecan is 111 nM with a polydispersity index of 0.04 and a drug load of 473 mg irinotecan HCl/mmol phospholipid [47]. All chemotherapeutics were given on days 0, 4 and 8. Saline was used as a vehicle control (Group 1) for the chemotherapeutics and its volume and administration routes used were the same as the volume used in the gemcitabine and nab-paclitaxel combination group (Group 2). The administration routes (IP or IV) for the chemotherapeutics were chosen based on previous reports [45,47]. For group 7 (nab-paclitaxel/gemcitabine followed by Sonazoid™), Sonazoid™ was included as a comparison to PS101 and was reconstituted according to the labelling instructions with water for injection. This group then received the same ultrasound regimen administration as the ACT-treated animals.

Table 1
Experimental groups.

Group	n	Treatment schedule
1. Saline followed by PS101	10	
2. Nab-paclitaxel/gemcitabine	9	
3. Nab-paclitaxel/gemcitabine followed by PS101	10	
4. PS101 followed by nab-paclitaxel/gemcitabine	10	Days 0, 4, 8
5. Liposomal irinotecan	9	
6. Liposomal irinotecan followed by PS101	10	
7. Nab-paclitaxel/gemcitabine followed by Sonazoid™	10	

2.5. ACT® setup and ultrasound administration

The experimental setup (Fig. 2A and B) comprises a heated VEVO animal imaging table (Visualsonics, Toronto, Canada) with a 5 mm thick layer of acoustic absorber material (Aptflex F48™, Precision Acoustics, Dorchester, UK). The surface temperature of the absorption plate was maintained at 37 °C. The absorbing material was used to suppress reflection of the ultrasound field from the table underneath the animal. Ultrasound coupling gel was used to acoustically couple the underside of the animal to the absorbing plate. A water-filled waveguide ending in a membrane was used to transmit ultrasound from the transducer to the mouse. The center of the acoustic field output was marked on the membrane to help position the animal underneath the bag. The transducer was custom made (Relab, Horten, Norway) and designed to output both 2.7 MHz and 0.5 Mhz pulses along the same acoustic axis. A driving pulse of 12-cycle sine wave of 2.7 MHz was used for the high frequency pulse with a pulse repetition frequency of 1 kHz and a 4-cycle sine wave of 0.5 MHz was used for the low frequency pulse with a pulse repetition frequency of 1 kHz. Both driving pulses were amplified with a power amplifier (Model number 2100 L Tomco Technologies, Stepney, Australia). The −3 dB beam diameters of the high frequency and low frequency pulses were 11 and 16 mm respectively at the operational distance of 20 cm from the transducer face. These were designed to cover and restrict the ultrasound fields to the subcutaneous tumors being treated [36]. For calibration of the 2.7 MHz and 0.5 MHz pulses pressure waveforms were recorded a priori in situ with a calibrated point hydrophone (Precision Acoustics, Dorchester, UK) placed in situ in the set-up at the location of the tumor volume center. A mechanical index value was calculated from the peak negative pressure of the waveforms using the equation $MI = \frac{p_r}{\sqrt{f_c}}$, where p_r is the peak rarefactional pressure in MPa, and f_c is the pulse center frequency in MHz. Note that the usual derating factor of 0.3 dB/cm/MHz was not applied as the intervening

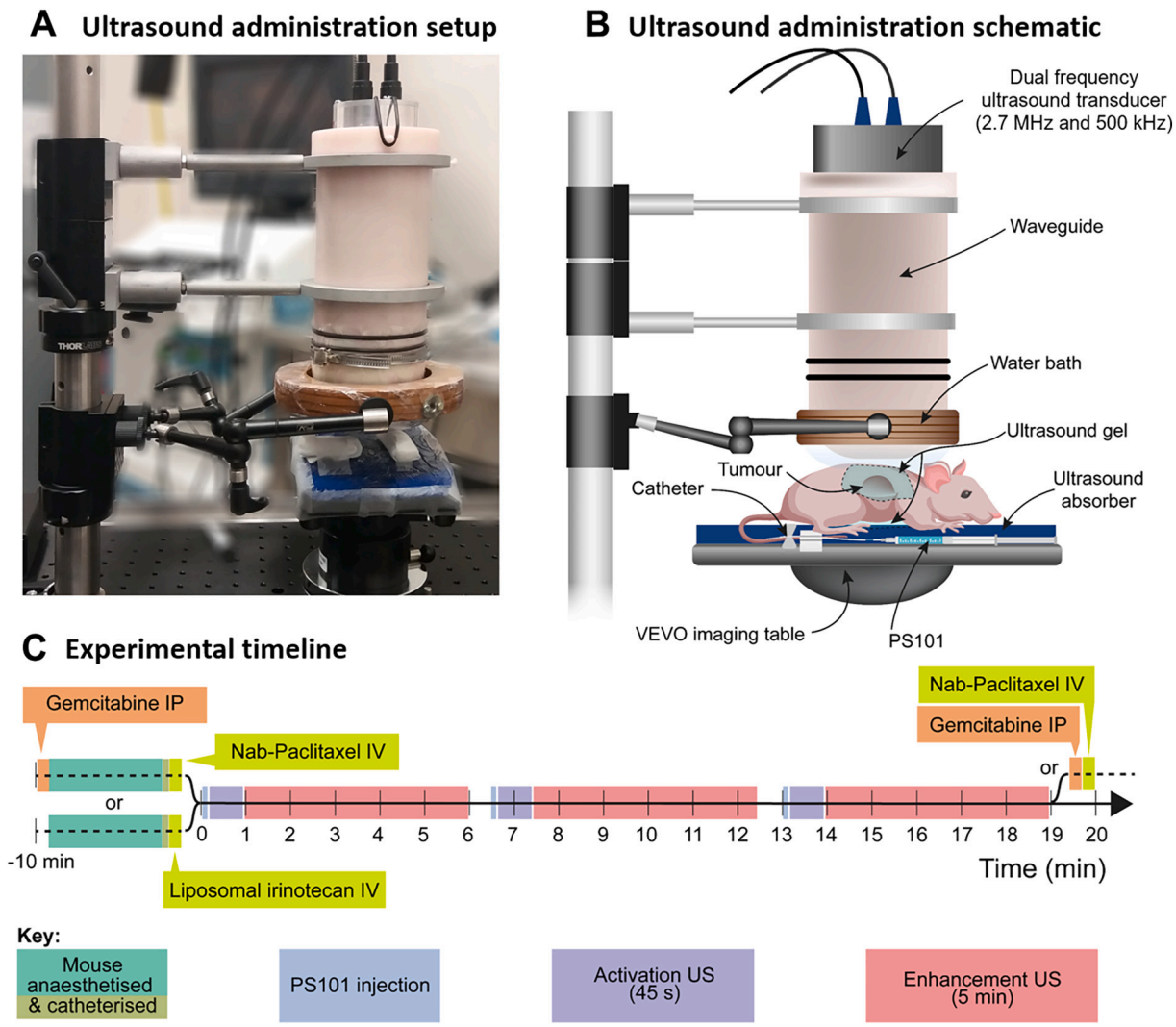

Fig. 2. Ultrasound administration setup and drug dosing timeline. A. Photograph of the ultrasound administration setup; B. Schematic depiction of the ultrasound administration setup; C. Experimental treatment timeline for groups that included PS101. The acoustic cluster therapy, which includes the injection of PS101, activation ultrasound, and enhancement ultrasound, was applied over a 19-min period either after or before the chemotherapeutics (gemcitabine/Nab-paclitaxel or liposomal irinotecan). IP, intraperitoneal; IV, intravenous; US, ultrasound.

media when treating the animals is water filled.

Mice were anesthetized by injecting a combination of acepromazine 3 mg/kg (Aceproject, Henry Schein, Dublin, OH, USA), ketamine 100 mg/kg (Ketathesia, Henry Schein, Dublin, OH, USA), and xylazine 10 mg/kg (Anased, Akorn Inc., Lakeforest, IL, USA), and catheterized in the lateral tail vein. The animals were placed onto the ultrasound absorber pad on the imaging table, taped in position and coupling gel applied before the waveguide was placed over the center of the tumor to be treated.

PS101 was administered via a 27G x 1/2“ winged infusion catheter set (Surflo, Terumo, Tokyo, Japan) attached to a 0.4mm fine bore polythene tubing with a 27G x 1/2” hypodermic needle fed into the open end, followed by a two-step ultrasound procedure of local activation (2.7 MHz for 45 s, 12 cycle pulse at 1 kHz pulse repetition frequency (PRF) and mechanical index (MI) 0.30) and enhancement (0.5 MHz for 5 min, 4 cycle pulse, 1 kHz PRF, MI 0.20). Three injections of PS101 followed by activation and enhancement ultrasound were performed for each treatment cycle.

The ultrasound and chemotherapy treatment schedule are depicted in Fig. 2C. Chemotherapeutics were administered either before or after insonation, determined according to treatment group. In groups where chemotherapy was administered before insonation, nab-paclitaxel and gemcitabine were administered immediately prior to insonation, after the animals were anesthetized and catheterized. In groups where chemotherapy was administered after insonation, nab-paclitaxel and gemcitabine were administered in the 20th minute following insonation.

2.6. *Tumor growth monitoring*

Tumors were measured using a caliper and tumor volumes were calculated using the formula $\frac{a \times b^2}{2}$, where ‘b’ is the smallest diameter and ‘a’ is the largest diameter. Up to Day 50, mice with tumors reaching an endpoint of tumor volume > 1500 mm^3 were sacrificed with regulated CO_2. On Day 50, animals with tumor volumes $\geq$60 mm^3 were sacrificed while those with tumor volumes $<$60 mm^3 were monitored for another 70 days. Mice that showed no visible sign of tumors at the end of the study (120 days) were considered complete responders. Tumors were collected from mice sacrificed on Day 50 or Day 120 and stained with hematoxylin and eosin (H&E) using the Leica ST5010 Autostainer XL system (Leica Biosystems Inc., Buffalo Grove, IL, USA). Experimental endpoints included tumor volume, percentage tumor inhibition on Day 50 comparing the chemotherapeutic plus PS101 groups with the corresponding chemotherapy only groups, proportion of complete responders, changes in body weight, and general observations of clinical

signs and acute effects.

2.7. Statistical analysis

For tumor volume on Day 50 the Anderson-Darling test of normality was used to determine the statistical significance in differences between groups. For groups that had a proportion of complete responders, bimodal distribution and non-parametric statistical tests were employed. Tumor volumes were plotted as median and interquartile range. The Kruskal-Wallis test was used for comparing multiple groups. The following five between-group comparisons were performed: group 3 versus group 2; group 4 versus group 2; group 7 versus group 2; group 3 versus group 4 and group 5 versus group 6. The two-stage linear step-up procedure described by Benjamini, Krieger and Yekutieli [48] was employed to control the false discovery rate (0.05) of these between group differences and reported as q values. Body mass was reported as mean ± standard error of the mean (SEM), and group differences were compared using parametric ANOVA.

Logistic regression was used to analyze the dependent variable complete response and the categorical variables drug type (liposomal irinotecan or nab-paclitaxel/gemcitabine) and PS101 (applied or not applied). Two models were compared, a main effects model and a main effects model with interaction between PS101 and drug. The best fit model was then chosen. *P*-values and odds ratios with 95% confidence interval (profile likelihood) were reported. A p-value <0.05 was considered statistically significant. All calculations were performed using Graphpad Prism version 9.2.0 (GraphPad Software Inc., San Diego, CA, USA).

3. Results

3.1. Tumor growth inhibition and between-group comparisons

The treatment regimens used in this study were well tolerated by the animals. No adverse effects of treatment were observed during or immediately after treatment. There was no loss of animals before the endpoint based on tumor volume.

The tumor volumes on Day 50 for the seven treatment groups along with their ranks based on the non-parametric Kruskall-Wallis test are shown in Fig. 3. The results of the Andersen-Darling test for normality are given in Table 2. The liposomal irinotecan and nab-paclitaxel/gemcitabine plus PS101 groups (groups 3–6) do not pass the test at the 0.05 level. Table 3 shows the results of Kruskal-Wallis test, for five between-group differences of interest calculated with false discovery rate set to 0.05. The q (corrected individual p) values are reported for the between-group differences throughout this study.

Changes in body mass are shown in Figs. 4B and 6B. During the treatment cycle there was a mean drop in body mass of no >5% in each group and the animals had returned to their original body weight on Day 17, three days after the last treatment (Day 14). The difference in body weights on Day 50 across all groups 1 to 7 is insignificant ($p = 0.6735$, ANOVA).

3.2. ACT® with nab-paclitaxel and gemcitabine

ACT® significantly improved the tumor growth inhibitory activity of nab-paclitaxel and gemcitabine. At 50 days, tumor volume was significantly lower in the nab-paclitaxel/gemcitabine followed by PS101 group compared to the nab-paclitaxel/gemcitabine alone group ($q = 0.0075$; Fig. 4A). The PS101 followed by nab-paclitaxel/gemcitabine treatment also resulted in a smaller mean tumor size, but the reduction was not statistically significant ($q = 0.2524$) when compared to the nab-paclitaxel/gemcitabine alone group. The PS101 followed by nab-paclitaxel/gemcitabine group was insignificantly different from the nab-paclitaxel/gemcitabine followed by PS101 group ($q = 0.0635$).

Compared with the nab-paclitaxel/gemcitabine alone group, tumor inhibition was 73% (median volume) in the PS101 followed by nab-paclitaxel/gemcitabine group, and 89% (median volume) in the nab-paclitaxel/gemcitabine followed by PS101 group on Day 50 (Fig. 4A and 4C). ACT® did not significantly affect the animals' body weight (Fig. 4B). Of the 20 mice treated with the nab-paclitaxel/gemcitabine and PS101 combination, 9 (45%) had complete tumor remission by 120 days, compared with 1 out of 9 (11%) of mice in the nab-paclitaxel/gemcitabine alone group (Fig. 4C).

Figure 5 shows representative images of hematoxylin and eosin (H&E) staining of tumor and residual tissues from mice treated with nab-paclitaxel/gemcitabine or nab-paclitaxel/gemcitabine plus PS101. Tissue samples were collected at the implantation site on Day 120 after the initiation of treatment. Pathological assessment suggested that most tumors consisted of a mix of viable tumor cells and necrotic regions as

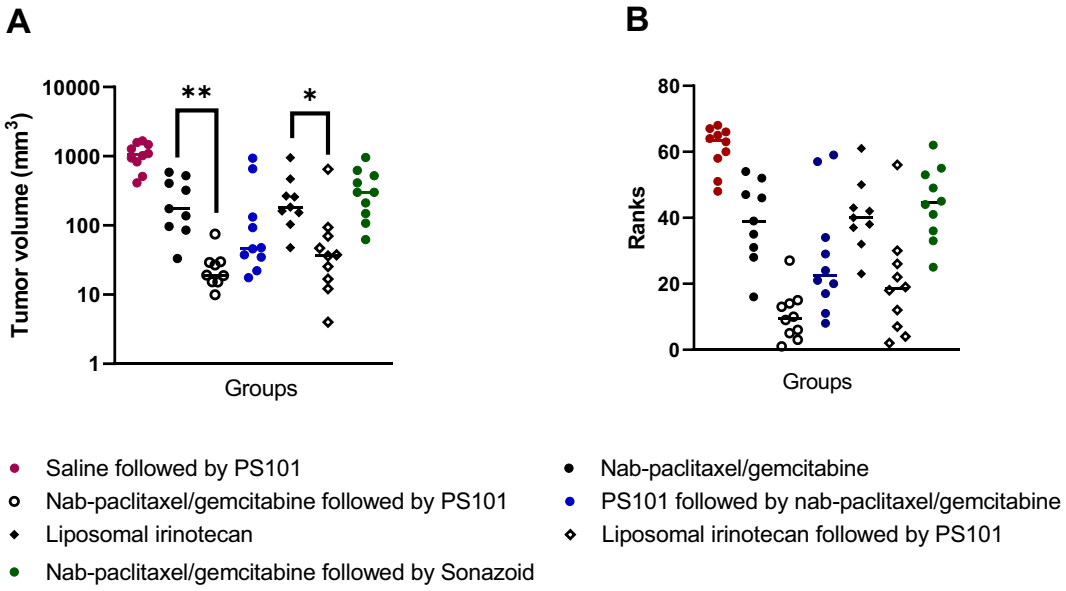

Fig. 3. Dot plot of individual animals by treatment groups for (A) tumor volume and (B) rank at Day 50. In (A), one animal in the PS101 followed by nab-paclitaxel/gemcitabine group has a tumor volume of 0 and is not displayed on the log plot of tumor volume. All treatments were significantly better than saline control. *, $p < 0.05$; **, $p < 0.01$.

Table 2
Anderson-Darling normality test for tumor volume on Day 50 for difference treatment groups.

Treatment Group[a]	1	2	3	4	5	6	7
p value	0.866	0.270	0.019	<0.0001	0.011	<0.0001	0.364
Pass[b]	Yes	Yes	No	No	No	No	Yes

[a] Group numbers are defined in Table 1.
[b] A p-value of <0.05 is considered to have failed the test.

Table 3
Between-group differences of tumor volume on Day 50, discovery, individual p and q values.

Comparison[a]	Discovery?	q value	Individual *p* value
Group 2 versus 3	Yes	0.0075	0.0018
Group 5 versus 6	Yes	0.0429	0.0204
Group 3 versus 4	No	0.0635	0.0453
Group 4 versus 2	No	0.2524	0.2404
Group 2 versus 7	No	0.4496	0.5352

[a] Group numbers are defined in Table 1.

well as chronic inflammation, but some complete responders where the tumors were reduced to either fatty tissue or fibrotic scar tissue were identified. A qualitative pathological assessment also confirmed that the tumors were representative of clinical PDAC. There were indications that nab-paclitaxel/gemcitabine plus PS101 treatment resulted in fewer tumor glands encompassed by scar-like tissues (dense stroma) compared to those nab-paclitaxel/gemcitabine treated tumors.

3.3. ACT® with liposomal irinotecan

ACT® also significantly improved the tumor growth inhibitory activity of liposomal irinotecan. At 50 days, tumor volume was significantly lower in the liposomal irinotecan followed by PS101 group than in the liposomal irinotecan alone group (q = 0.0429; Fig. 6A).

Compared with the liposomal irinotecan alone group, tumor inhibition was 80% (median volume) in the liposomal irinotecan followed by PS101 group (Fig. 6A and 6C). ACT® treatment did not significantly affect the animals' body weight (Fig. 6B). Of the 10 mice treated with the liposomal irinotecan and PS101 combination, 5 (50%) had complete tumor remission by 120 days, compared with 1 out of 9 (11%) of mice in the liposomal irinotecan alone group (Fig. 6C).

Figure 7 shows representative H&E staining of tumor and residual tissues from mice treated with liposomal irinotecan or liposomal irinotecan plus PS101. Tissue samples were collected at the implantation site on Day 120 after the initiation of treatment. In the liposomal irinotecan and PS101 combination group, all the animals evaluated by pathology were complete responders and had only adipose tissues whereas tissues from mice treated with liposomal irinotecan alone had multiple tumor glands with dense stroma.

3.4. Logistic regression analysis of complete responses

Logistic regression was used to determine whether the complete response rates observed in the ACT-based combination regimen were significantly higher than that seen with the chemotherapy alone regimens. A main effects model for the dependent variable complete response with categorical variables drug and PS101 was designated model 1. This was compared against the main effects with an additional drug and PS101 interaction term, model 2. The *p* value for model comparison (likelihood ratio test) was 0.9054 (insignificant), hence the main effects, model 1, was selected. The p value for β_1: drug was 0.8183 (insignificant). There was a significant p value for β_2: ACT® of 0.0195. The odds of complete response are 7.2 (95% confidence interval from 1.622 to 51.77) times higher for regimens with PS101 treatment than those without ACT® treatment (Table 4) suggesting a substantial benefit of ACT® in addition to SoC.

4. Discussion and conclusions

ACT® is a novel technology which, based on our results, is potentially capable of improving treatment outcomes in PDAC, a malignancy notoriously resistant to treatment with current therapeutic options. Previous studies of ACT® have demonstrated promising results in cell-line xenograft mouse models of several cancer types [30,32,34,41,42]. We previously demonstrated that ACT® in combination with paclitaxel provided significant reductions in tumor volume in PDAC cell-line based mouse xenograft models [42]. However, cell-line based xenograft models lack the dense stroma that is often observed in human PDAC. As dense stroma is thought to be a major factor in therapeutic resistance in PDAC, models that better represent PDAC stroma are needed to demonstrate the utility of ACT® technology. In this study we used a PDX model to evaluate the effectiveness of ACT® in enhancing the effect of chemotherapeutic agents currently being used for treating patients with PDAC. PDX models are thought to provide a better representation of the histopathology and molecular features of the original tumor than cell-derived xenograft models [43]. Pathological analysis of H&*E*-stained sections verified that our PDX model contained dense stroma as seen in PDAC patient tumors.

In this study we found that ACT® significantly improved the therapeutic efficacy of both nab-paclitaxel/gemcitabine and liposomal irinotecan. These drugs are cornerstones in the management of PDAC. The best treatment regimens were when drug administration proceeded ACT® treament, but interestingly the anti-tumor effect was almost maintained when the drugs were administered after ACT®-treatment was finalized. Similar observations have been made in previous work [32] with ACT® combined with irinotecan. This shows that the effect of ACT® is not dominated onto the drug itself, but rather affects the vasculature and tumor microenvironment to facilitate drug delivery and/or therapeutic response. Sonoporation, as described previously [49], typically proposes methods with in situ actions onto a drug or modes of action that requires the presence of a drug. For the ACT proceeded by drug treatment group, cell membrane pore formation during ACT treatment would have resealed (with duration in the order of a minute [50]) before exposure to the drug. It has been shown here that ACT® has a significant contribution from different modes of action and has effect on the tumor microenvironment independent of the drug and this could explain the improved effect of ACT compared to Sonazoid™ (Fig. 4). This is promising as it suggests that ACT® could also potentially improve the delivery and effect of other cancer therapeutics. However, the effect of the modulation of tumor microenvironment on the metastatic spread of tumor remains to be investigated.

A numerically greater proportion of mice achieved complete tumor remission at 120 days with ACT® combined with chemotherapeutics compared with chemotherapeutics alone (for both the nab-paclitaxel plus gemcitabine and liposomal irinotecan regimens), further supporting the conclusion that ACT® significantly improves the antitumor activity of chemotherapeutics in PDAC. The evaluated regimens of chemotherapy both consist of macromolecules or nanomedicine. These formulations have advantages over the traditional formulations in terms of toxicity profile and possibly tumor retention [51]. However, biological barriers such as the blood vessel wall and extracellular matrix limit the penetration and effect of these drugs [52]. While the exact mode of

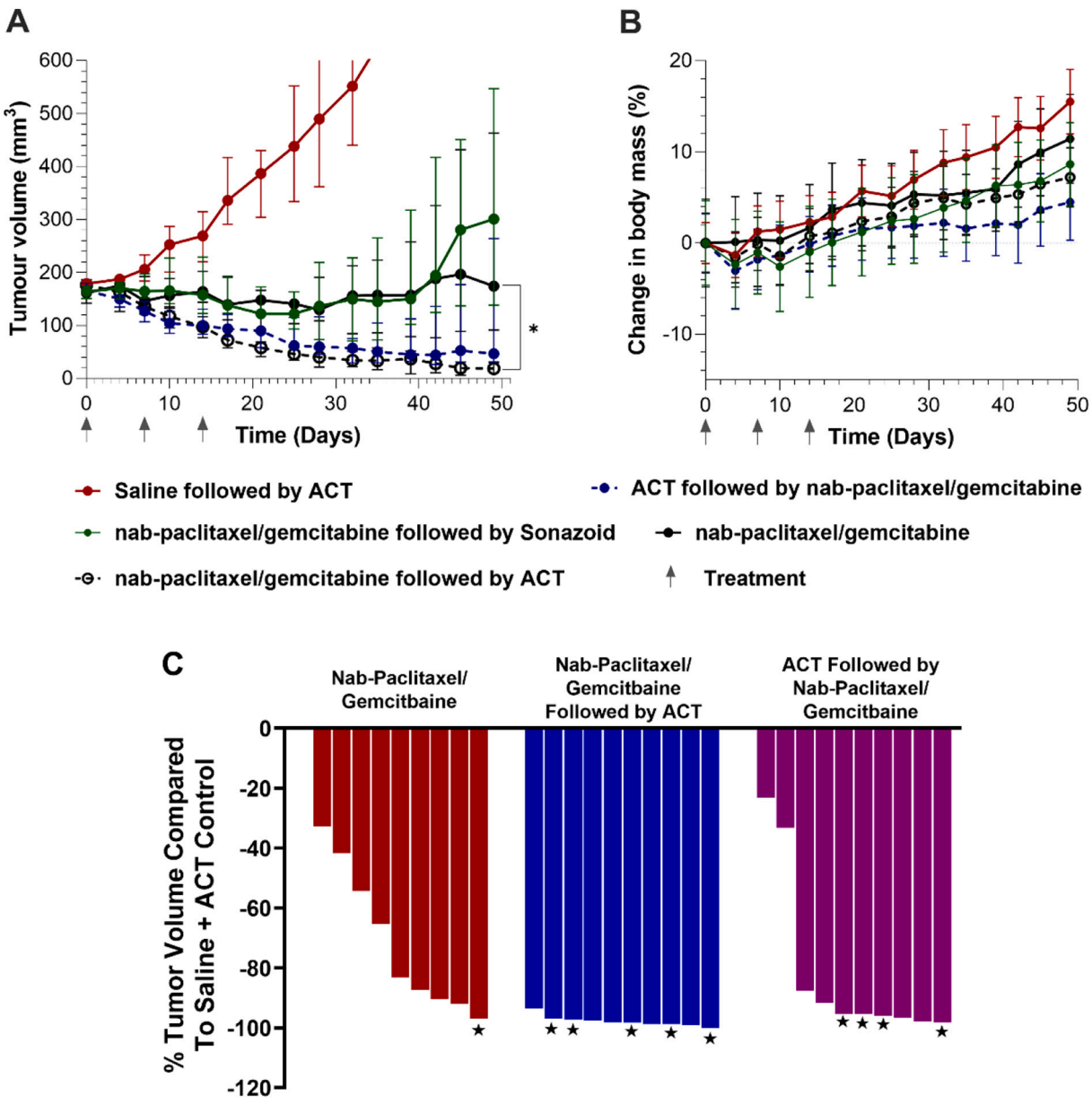

Fig. 4. Effect of ACT® on tumor volume and body weight in mice treated with nab-paclitaxel and gemcitabine. A) Tumor growth curves. B) Mouse body weight changes. C) Percent tumor volume reduction on Day 50 compared to saline plus ACT® control group. Nab-paclitaxel followed by ACT® was significantly better than nab-paclitaxel alone ($p = 0.0018$). *, $p = 0.0018$. ★, Complete responders at Day 120. ACT®, acoustic cluster therapy. Number of mice enrolled in each group is listed in Table 1.

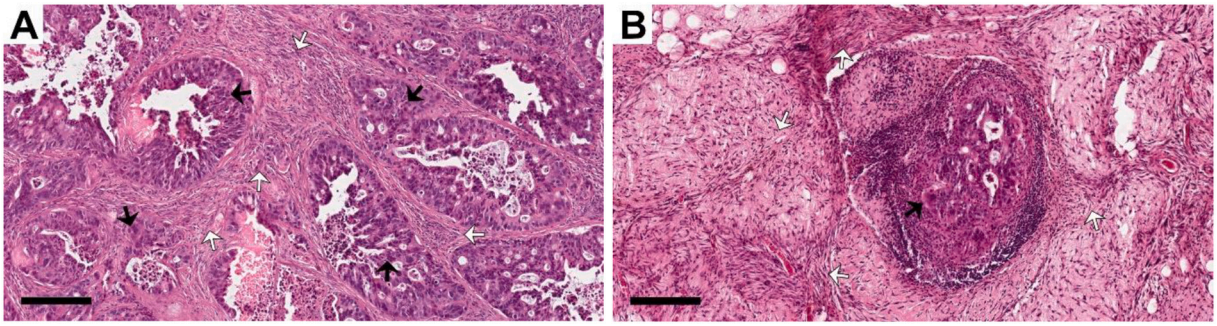

Fig. 5. Hematoxylin and eosin staining of tumor and residual tissues from mice treated with nab-paclitaxel/gemcitabine (A) or nab-paclitaxel/gemcitabine plus PS101 (B) regimen. Solid arrows indicate tumor glands and open arrows indicate dense stroma (A) or fibrotic tissues (B). Scale bar = 200 μM.

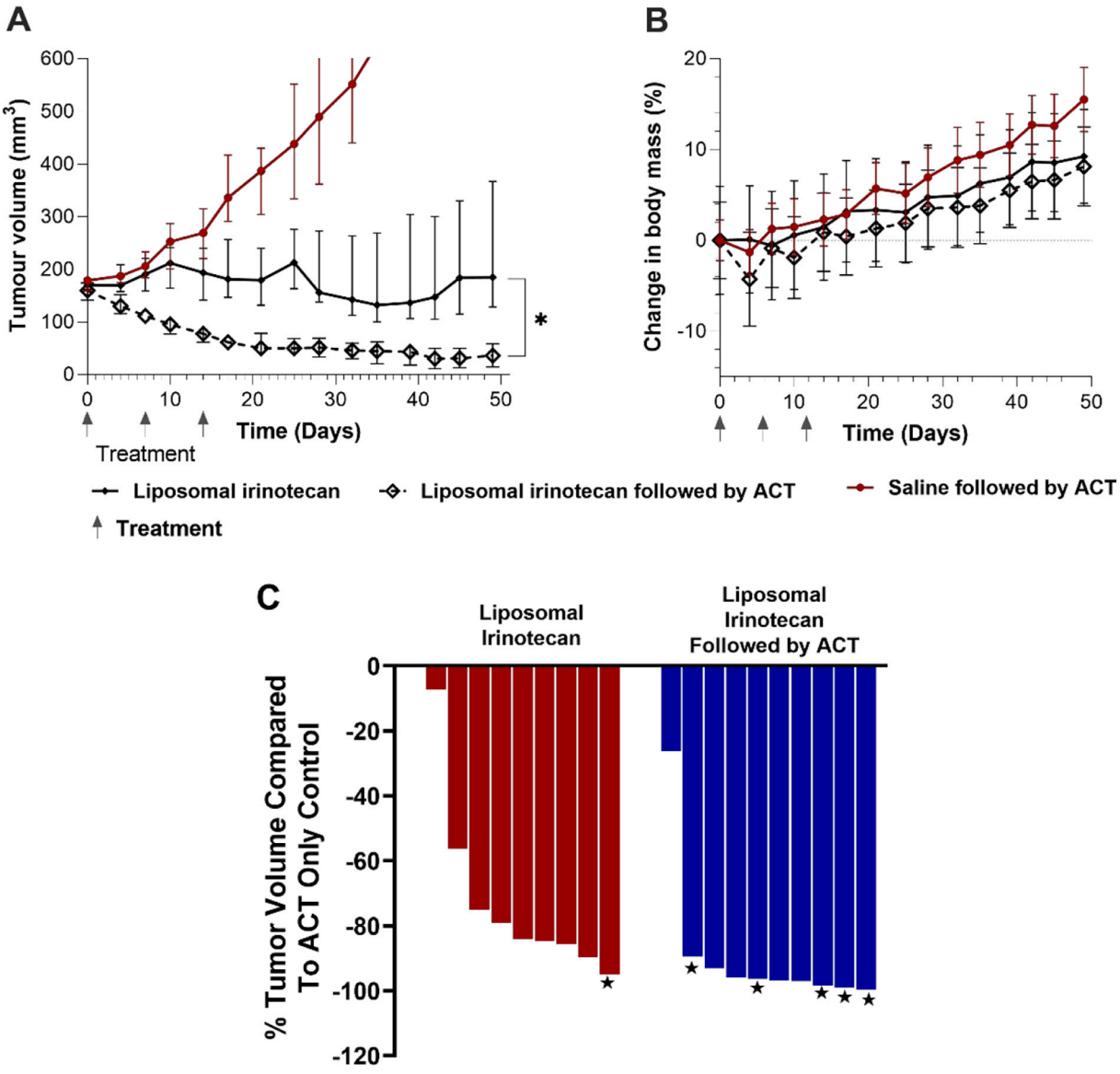

Fig. 6. Effect of ACT® on tumor volume and body weight in mice treated with liposomal irinotecan. A) Tumor growth curves. B) Mouse body weight curves. C) Percent tumor volume reduction compared to saline and ACT control group on Day 50. *p = 0.0429. ★, Complete responders at Day 120. ACT®, acoustic cluster therapy. Number of mice enrolled in each group is listed in Table 1.

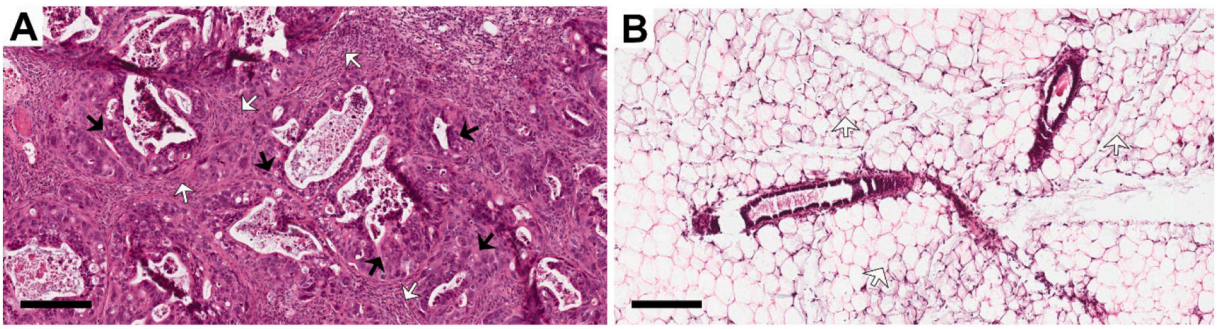

Fig. 7. hematoxylin and eosin staining of tumor and residual tissues from mice treated with liposomal irinotecan with (A) or without (B) PS101. Solid arrows indicate tumor glands. Open arrows indicate dense stroma (A) or residual adipose tissues (B).

action for ACT® is not clear, we consider both vascular and peri-vascular transport due to the oscillations of ACT® to be likely effects and it is therefore possible that these nanosized drugs benefit especially from ACT®.

In conclusion, this study demonstrates that ACT® can significantly enhance the antitumor activity (both tumor growth inhibition and

Table 4
Results of logistic regression main effects model with dependent variable complete response, and categorical variables PS101 and chemotherapeutics.

Predictor	β	SE β	p value	Odds ratio	95% CI
Intercept	−2.161	0.8347	0.0096	0.1152	0.01595 to 0.4811
Drug	0.1584	0.6894	0.8183	1.172	0.2983 to 4.642
PS101	1.975	0.8457	0.0195	7.204	1.622 to 51.77

SE, standard error; CI, confidence interval.

complete response rate) of two chemotherapeutic regimens (nab-paclitaxel/gemcitabine and liposomal irinotecan) in a patient-derived xenograft mouse model of PDAC. As both the nab-paclitaxel/gemcitabine and liposomal irinotecan regimens are SoC treatments approved by the USA FDA for patients with advanced PDAC, this study provides strong preclinical evidence supporting the clinical testing of ACT-based regimens in patients. Based on the results from this study, an expansion cohort with metastatic PDAC is being considered for an ongoing Phase I clinical study of ACT® in patients with advanced solid tumors with liver metastases [53]. This trial could clinically validate the findings from this study; its results are therefore awaited with great interest.

Funding

The study was partially funded through a Research grant by the Norwegian Research Council (NRC grant number 269818) and Innovasjonsrammen 2017 through Norwegian Innovation. EXACT Therapeutics provided laboratory support and set up, data analysis, interpretation of the data, and review of the manuscript. It also funded the development of this publication including medical writing and editorial assistance.

Data availability

Data will be made available on request.

Acknowledgements

We would like to thank Kimberly Brothers and Pawan Noel for their technical support for the animal studies and Jennifer Green (Green Ink Communications Ltd., UK) for providing medical writing and editorial assistance towards the development of this article.

References

[1] R.L. Siegel, et al., Cancer statistics, 2021, CA Cancer J. Clin. 71 (1) (2021) 7–33.
[2] American Cancer Society, Key Statistics for Pancreatic Cancer, Available at, https://www.cancer.org/cancer/pancreatic-cancer/about/key-statistics.html, 2021 [Accessed 19 June 2021].
[3] American Cancer Society, Cancer Statistics Center, Estimates, 2021. Available at, https://cancerstatisticscenter.cancer.org [Accessed 19 June 2021].
[4] L. Rahib, et al., Estimated projection of US Cancer incidence and death to 2040, JAMA Netw. Open 4 (4) (2021), e214708.
[5] T. Conroy, et al., FOLFIRINOX versus gemcitabine for metastatic pancreatic Cancer, N. Engl. J. Med. 364 (19) (2011) 1817–1825.
[6] D.D. Von Hoff, et al., Increased survival in pancreatic cancer with nab-paclitaxel plus gemcitabine, N. Engl. J. Med. 369 (18) (2013) 1691–1703.
[7] A. Wang-Gillam, et al., Nanoliposomal irinotecan with fluorouracil and folinic acid in metastatic pancreatic cancer after previous gemcitabine-based therapy (NAPOLI-1): a global, randomised, open-label, phase 3 trial, Lancet 387 (10018) (2016) 545–557.
[8] Y. Boucher, L.T. Baxter, R.K. Jain, Interstitial pressure gradients in tissue-isolated and subcutaneous tumors: implications for therapy, Cancer Res. 50 (15) (1990) 4478–4484.
[9] C.H. Heldin, et al., High interstitial fluid pressure - an obstacle in cancer therapy, Nat. Rev. Cancer 4 (10) (2004) 806–813.
[10] D. Mahadevan, D.D. Von Hoff, Tumor-stroma interactions in pancreatic ductal adenocarcinoma, Mol. Cancer Ther. 6 (4) (2007) 1186–1197.
[11] A.I. Minchinton, I.F. Tannock, Drug penetration in solid tumours, Nat. Rev. Cancer 6 (8) (2006) 583–592.
[12] P.P. Provenzano, et al., Enzymatic targeting of the stroma ablates physical barriers to treatment of pancreatic ductal adenocarcinoma, Cancer Cell 21 (3) (2012) 418–429.
[13] D.D. Von Hoff, R. Korn, S. Mousses, Pancreatic cancer–could it be that simple? A different context of vulnerability, Cancer Cell 16 (1) (2009) 7–8.
[14] B. Diop-Frimpong, et al., Losartan inhibits collagen I synthesis and improves the distribution and efficacy of nanotherapeutics in tumors, Proc. Natl. Acad. Sci. U. S. A. 108 (7) (2011) 2909–2914.
[15] V. Kumar, et al., Noninvasive assessment of losartan-induced increase in functional microvasculature and drug delivery in pancreatic ductal adenocarcinoma, Transl. Oncol. 9 (5) (2016) 431–437.
[16] S. Suklabaidya, et al., Experimental models of pancreatic cancer desmoplasia, Lab. Investig. 98 (1) (2018) 27–40.
[17] J. Unga, M. Hashida, Ultrasound induced cancer immunotherapy, Adv. Drug Deliv. Rev. 72 (2014) 144–153.
[18] K.H. Martin, P.A. Dayton, Current status and prospects for microbubbles in ultrasound theranostics, Wiley Interdiscip. Rev. Nanomed. Nanobiotechnol. 5 (4) (2013) 329–345.
[19] J.M. Tsutsui, F. Xie, R.T. Porter, The use of microbubbles to target drug delivery, Cardiovasc. Ultrasound 2 (2004) 23.
[20] S. Snipstad, et al., Sonopermeation to improve drug delivery to tumors: from fundamental understanding to clinical translation, Expert Opin. Drug Deliv. 15 (12) (2018) 1249–1261.
[21] L.J. Delaney, et al., Making waves: how ultrasound-targeted drug delivery is changing pharmaceutical approaches, Mater. Adv. 3 (2022) 3023–3040.
[22] G. Dimcevski, et al., A human clinical trial using ultrasound and microbubbles to enhance gemcitabine treatment of inoperable pancreatic cancer, J. Control. Release 243 (2016) 172–181.
[23] A. Rix, et al., Effects of contrast-enhanced ultrasound treatment on neoadjuvant chemotherapy in breast cancer, Theranostics 11 (19) (2021) 9557–9570.
[24] A. Carpentier, et al., Clinical trial of blood-brain barrier disruption by pulsed ultrasound, Sci. Transl. Med. 8 (343) (2016) 343re2.
[25] J. Gao, et al., An ultrasound responsive microbubble-liposome conjugate for targeted irinotecan-oxaliplatin treatment of pancreatic cancer, Eur. J. Pharm. Biopharm. 157 (2020) 233–240.
[26] J. Gao, et al., A single microbubble formulation carrying 5-fluorouridine, irinotecan and oxaliplatin to enable FOLFIRINOX treatment of pancreatic and colon cancer using ultrasound targeted microbubble destruction, J. Control. Release 338 (2021) 358–366.
[27] P. Dwivedi, et al., Magnetic targeting and ultrasound activation of liposome-microbubble conjugate for enhanced delivery of anticancer therapies, ACS Appl. Mater. Interfaces 12 (21) (2020) 23737–23751.
[28] T. Li, et al., Pulsed high-intensity focused ultrasound enhances delivery of doxorubicin in a preclinical model of pancreatic Cancer, Cancer Res. 75 (18) (2015) 3738–3746.
[29] M.H. Yu, et al., Therapeutic effects of microbubbles added to combined high-intensity focused ultrasound and chemotherapy in a pancreatic Cancer xenograft model, Korean J. Radiol. 17 (5) (2016) 779–788.
[30] N. Bush, et al., Theranostic attributes of acoustic cluster therapy and its use for enhancing the effectiveness of liposomal doxorubicin treatment of human triple negative breast cancer in mice, Front. Pharmacol. 11 (2020) 75.
[31] K. Kooiman, et al., Acoustic behavior of microbubbles and implications for drug delivery, Adv. Drug Deliv. Rev. 72 (2014) 28–48.
[32] N. Bush, et al., Therapeutic dose response of acoustic cluster therapy in combination with irinotecan for the treatment of human colon cancer in mice, Front. Pharmacol. 10 (2019) 1299.
[33] A.J. Healey, et al., Acoustic cluster therapy: in vitro and ex vivo measurement of activated bubble size distribution and temporal dynamics, Ultrasound Med. Biol. 42 (5) (2016) 1145–1166.
[34] A. van Wamel, et al., Acoustic cluster therapy (ACT) - pre-clinical proof of principle for local drug delivery and enhanced uptake, J. Control. Release 224 (2016) 158–164.
[35] A. van Wamel, et al., Acoustic cluster therapy (ACT) enhances the therapeutic efficacy of paclitaxel and Abraxane® for treatment of human prostate adenocarcinoma in mice, J. Control. Release 236 (2016) 15–21.
[36] K.K. Andersen, et al., A harmonic dual-frequency transducer for acoustic cluster therapy, Ultrasound Med. Biol. 45 (9) (2019) 2381–2390.
[37] P. Sontum, et al., Acoustic Cluster Therapy (ACT)–A novel concept for ultrasound mediated, targeted drug delivery, Int. J. Pharm. 495 (2) (2015) 1019–1027.
[38] O. Myhre, et al., Safety assessment in rats and dogs of acoustic cluster therapy, a novel concept for ultrasound mediated, targeted drug delivery, Pharmacol. Res. Perspect. 4 (6) (2016), e00274.
[39] A.K. Åslund, et al., Efficient enhancement of blood-brain barrier permeability using acoustic cluster therapy (ACT), Theranostics 7 (1) (2017) 23–30.
[40] M. Olsman, et al., Acoustic cluster therapy (ACT®) enhances accumulation of polymeric micelles in the murine brain, J. Control. Release 337 (2021) 285–295.
[41] A. van Wamel, et al., Acoustic cluster therapy (ACT) enhances the therapeutic efficacy of paclitaxel and Abraxane(R) for treatment of human prostate adenocarcinoma in mice, J. Control. Release 236 (2016) 15–21.
[42] S. Kotopoulis, et al., Sonoporation with acoustic cluster therapy (ACT(R)) induces transient tumour volume reduction in a subcutaneous xenograft model of pancreatic ductal adenocarcinoma, J. Control. Release 245 (2017) 70–80.
[43] A. Kamili, et al., Accelerating development of high-risk neuroblastoma patient-derived xenograft models for preclinical testing and personalised therapy, Br. J. Cancer 122 (5) (2020) 680–691.
[44] S. Gummadi, J.R. Eisenbrey, A. Lyshchik, Contrast-enhanced ultrasonography in interventional oncology, Abdom. Radiol. (NY) 43 (11) (2018) 3166–3175.
[45] P. Noel, et al., Triptolide targets super-enhancer networks in pancreatic cancer cells and cancer-associated fibroblasts, Oncogenesis 9 (11) (2020) 100.

[46] D.C. Drummond, et al., Development of a highly active nanoliposomal irinotecan using a novel intraliposomal stabilization strategy, Cancer Res. 66 (6) (2006) 3271–3277.
[47] A.V. Kalra, et al., Preclinical activity of nanoliposomal irinotecan is governed by tumor deposition and intratumor prodrug conversion, Cancer Res. 74 (23) (2014) 7003–7013.
[48] Y. Benjamini, A.M. Krieger, D. Yekutieli, Adaptive linear step-up procedures that control the false discovery rate, Biometrika 93 (2006) 491–507.
[49] S. Snipstad, et al., Sonopermeation to improve drug delivery to tumors: from fundamental understanding to clinical translation, Expert. Opin. Drug Deliv. 15 (12) (2018) 1249–1261.
[50] Y. Hu, J.M.F. Wan, A.C.H. Yu, Membrane perforation and recovery dynamics in microbubble-mediated sonoporation, Ultrasound Med. Biol. 39 (12) (2013) 2393–2405.
[51] R. van der Meel, et al., Smart cancer nanomedicine, Nat. Nanotechnol. 14 (11) (2019) 1007–1017.
[52] S. Snipstad, et al., Ultrasound and microbubbles to beat barriers in tumors: improving delivery of nanomedicine, Adv. Drug Deliv. Rev. 177 (2021), 113847.
[53] U. Banerji, et al., Phase I trial of acoustic cluster therapy (ACT) with chemotherapy in patients with liver metastases of gastrointestinal origin (ACTIVATE study), J. Clin. Oncol. 39 (15_suppl) (2021), https://doi.org/10.1200/JCO.2021.39.15_suppl.TPS3145.